Capacitance Spectroscopy for Quantifying Recombination Losses in Nonfullerene Small-Molecule Bulk Heterojunction Solar Cells

Viktor V. Brus, Christopher M. Proctor, Niva A. Ran, and Thuc-Quyen Nguyen**

The light intensity dependence of the main photoelectrical parameters of the nonfullerene small-molecule bulk heterojunction (BHJ) solar cells p-DTS(FBTTh$_2$)$_2$:perylene diimide (T1:PDI) shows that the nongeminate recombination losses play an important role in this system. A simple approach for the quantitative analysis of capacitance spectroscopy data of the organic BHJ solar cells, which allows to determine the density of free charge carriers as a function of applied bias under standard working conditions, is demonstrated. Using the proposed capacitance spectroscopic technique, the nongeminate recombination losses in the T1:PDI solar cells are quantitatively characterized in the scope of the bimolecular- and trap-assisted recombination mechanisms. Their contributions are separately analyzed within a wide range of the applied bias.

1. Introduction

The continually growing efficiency and stability of solution-processed organic bulk heterojunction (BHJ) solar cells make them attractive for a wide range of applications.[1–5] The active layer of organic BHJ solar cells consists of a nanostructured blend of electron-donating and -accepting materials. Great attention has been paid to the development and optimization of different donor materials blended with fullerene acceptors such as phenyl-C61-butyric acid methyl ester (PCBM).[6–8] PCBM has been shown to have optimal electrical properties for solar cell performance. However, its intensive solvent and energy consuming production is cost prohibitive and may limit large scale production.[9] Therefore, the development, application, and characterization of new nonfullerene low-cost acceptor materials in BHJ solar cells are very important. Despite this importance, there has been little work done to develop nonfullerene acceptors, and in particular the loss mechanisms that limit their performance in organic BHJ solar cells remains poorly understood.[10]

The low-cost electron acceptor material perylene diimide (PDI) possesses high electron affinity, large extinction coefficient, and relatively high electron mobility, which makes it a good candidate for application in nonfullerene organic solar cells.[11] The p-DTS(FBTTh$_2$)$_2$:perylene diimide (T1:PDI) small-molecule system with 1,8-diiodooctane (DIO) additive was reported for the first time 2 years ago as one of the most efficient nonfullerene BHJ solar cells at that time.[12] It was found that the relatively low efficiency of charge separation due to the geminate recombination in the T1:PDI system is one of the main reasons for the lower photovoltaic efficiency as compared to conventional fullerene-based T1:PCBM system.[13] However, the charge transport in PDI was shown to be dominated by trapping.[14] The presence of deep traps can cause additional nongeminate recombination losses in the T1:PDI system.

Recently a technique has been developed for the determination of the density of free charge carriers and nongeminate recombination losses in BHJ solar cells from the analysis of their voltage-impedance characteristics in the dark and under illumination.[15] Impedance spectroscopy is a nondestructive tool for the investigation of different inorganic and organic heterojunction solar cells.[16–20] This method allows for the analysis of electrical processes in heterojunction solar cells under working conditions. The measured impedance spectra of organic BHJ solar cells, in some cases, can be analyzed in the scope of a simple equivalent circuit: a resistor in series with a resistor and capacitor connected in parallel, which represent the series resistance originated from the contact resistance and the conductance and the capacitance of the BHJ layer, respectively.[15] Unfortunately, not all organic BHJ solar cells can be described by a simple equivalent circuit. In particular the impedance response of the T1:PDI BHJ solar cell under consideration cannot be accurately modeled using such a simple equivalent circuit model. More advanced and complicated equivalent circuits should be developed for the description of the measured spectra. Therefore, in the case of organic solar cells, which do not show standard AC characteristics, the direct analysis of impedance spectroscopy is complex and not straightforward. Here, we propose a simple approach for the determination of the density of free charge carriers and thus nongeminate recombination losses in BHJ solar cells based on the analysis of their capacitance spectra, which is readily adaptable for practical application. First a quantitative model for the capacitance spectroscopy of BHJ solar cells will be presented

Dr. V. V. Brus, Dr. C. M. Proctor, N. A. Ran, Prof. T.-Q. Nguyen
Center for Polymers and Organic Solids
Department of Chemistry and Biochemistry
University of California at Santa Barbara
Santa Barbara, CA 93106, USA
E-mail: vbrus@chem.ucsb.edu; quyen@chem.ucsb.edu

DOI: 10.1002/aenm.201502250

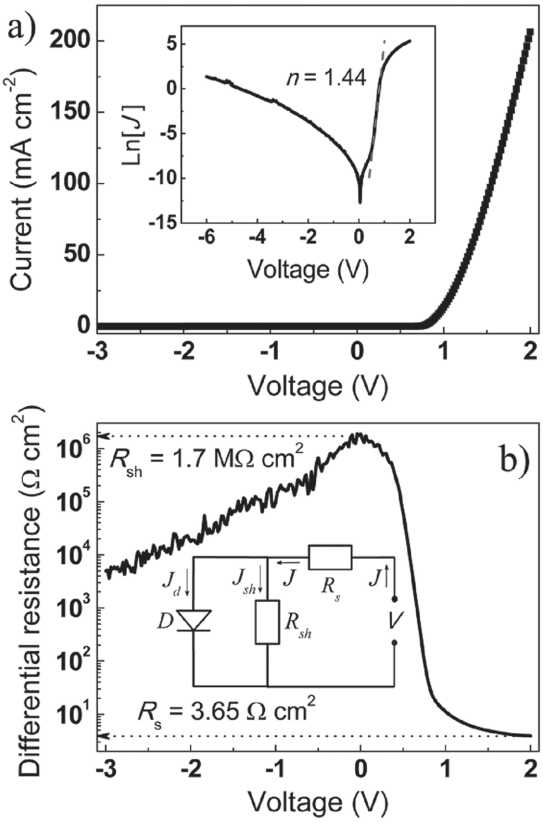

Figure 1. a) Dark *J–V* characteristic of the T1:PDI solar cell, measured at 300 K; b) Differential resistance of the solar cell in the dark vs applied bias (the inset shows the DC equivalent circuit of the solar cells in the dark).

and then applied to determine the dielectric constant and the density of free charge carriers in the T1:PDI small-molecule (SM) BHJ solar cells under standard 1.5AM 100 mW cm^{-2} illumination conditions at different biases. Afterwards, the determined dielectric constant and voltage dependence of the density of free charge carriers will be used for the quantitative analysis of the nongeminate recombination losses in the T1:PDI SM BHJ solar cells in the scope of the bimolecular and trap assisted recombination mechanisms.

2. Results and Discussions

2.1. *J–V* Characteristics in the Dark

Figure 1a shows the current density–voltage (*J–V*) characteristics of the T1:PDI solar cell at 300 K in the dark. The measured *J–V* curve can be described by the following empirical equation:

$$J = J_0\left(\exp\left(\frac{q(V-JR_s)}{nkT}\right)-1\right)+\frac{V-JR_s}{R_{sh}} = J_d + J_{sh} \quad (1)$$

where J_0 is the saturation current density, n is the ideality coefficient, and R_s and R_{sh} are the series and shunt resistance, respectively. If the value of the ideality coefficient n is larger than unity, it may be a sign of the presence of electrically active traps.[21–23] The values of R_s and R_{sh} resistance of the solar cell can be determined from the voltage dependence of the differential resistance $R_{diff} = \Delta V/\Delta J$ as shown in Figure 1b.

It is seen that the differential resistance decreases exponentially as the forward bias is increased. If the applied forward bias is further increased the $R_{dif}(V)$ curve saturates (the applied external electric field compensates for the rectifying potential barrier between the cathode and anode electrodes and the current through the solar cell is limited only by its series resistance R_s). Therefore, the value of R_s can be determined by the extrapolation of the saturated part of the R_{dif} (V) curve toward the interception with the resistance axis. The value of the shunt resistance R_{sh} is equal to the differential resistance in the vicinity of zero bias.[23,24]

The light intensity dependence of *J–V* characteristics is a simple method for the analysis of dominating recombination mechanisms in organic BHJ solar cells.[25–28] **Figure 2**a shows the *J–V* characteristics of the T1:PDI solar cell measured at different white light intensities. The values of the main photoelectrical characteristics of the solar cell under standard 1.5 AM 100 mW cm^{-2} illumination are also given in Figure 2a. The short-circuit current J_{sc} vs light intensity dependence is almost perfectly linear (Figure 2b) suggesting only a small contribution of the bimolecular recombination losses under short-circuit conditions. However, the slope of the V_{oc} vs light intensity dependence is larger than kT/q with a value of 1.18 kT/q (Figure 2c). This is evidence of the presence of trap-assisted Shockley-Read-Hall (SRH) recombination via deep traps, which are efficient recombination centers (the probability of recombination is higher than that of detrapping),[29] in addition to bimolecular recombination which is known to dominate at open-circuit conditions in most BHJ solar cells with fullerene acceptors.[30] Figure 2d shows the fill factor *FF* vs light intensity dependence. Geminate recombination is independent of charge carrier density and thus its rate is light intensity independent. However, the nongeminate recombination rate increases with the increase of charge carrier density. The decrease of *FF* with increasing light intensity shows that the nongeminate recombination losses play an important role in the T1:PDI system and, thus, their detailed quantitative characterization under different condition is of a great practical interest.

From the light intensity dependence, it is clear that both bimolecular and SRH recombination mechanisms should be considered in order to describe the nongeminate recombination losses in the T1:PDI SM BHJ solar cells. The bimolecular and SRH recombination rates are governed by Equations (2) and (3), respectively:[31–33]

$$R_{BMR} = \frac{q}{\varepsilon\varepsilon_0}\xi\left(\mu_n+\mu_p\right)n^2 \quad (2)$$

$$R_{SRH} = \frac{C_nC_pN_t}{\left(C_p+C_n\right)}n = \frac{q}{\varepsilon\varepsilon_0}\mu_pN_tn, \quad (3)$$

where ε is the dielectric constant of the BHJ layer, ε_0 is the permittivity of free space, ξ is the Langevin prefactor, μ_n and μ_p are the electron and hole mobilities, n is the density of free charge carriers, C_n and C_p are the capture coefficients for electrons and

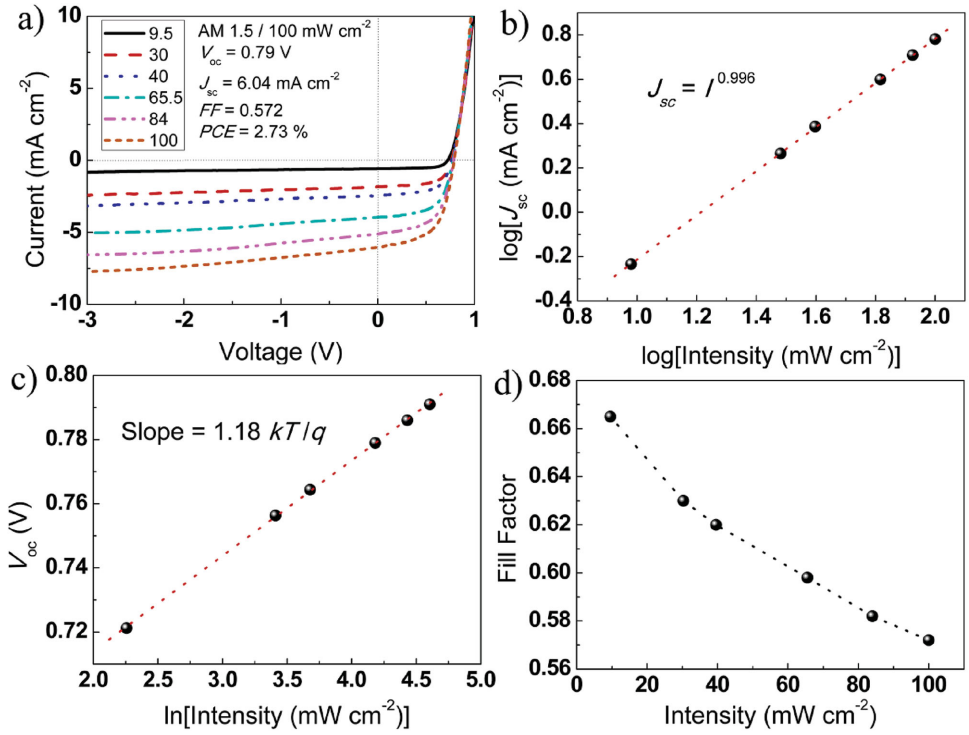

Figure 2. a) *J–V* curves of the T1:PDI solar cell under different white light illumination conditions (illumination intensity is measured in mW cm^{-2}); b) The short-circuit current vs light intensity dependence; c) The open-circuit voltage vs light intensity dependence; d) The fill factor vs light intensity dependence.

holes, respectively, and N_t is the density of deep traps. Taking into account Equations (2) and (3) we can write the expression for the recombination current J_{rec} in the solar cells under investigation:

$$J_{rec} = qL(R_{BMR} + R_{SRH}) = \frac{q^2 L}{\varepsilon\varepsilon_0}\left[\xi(\mu_n + \mu_p)n^2 + \mu_p N_t n\right] \quad (4)$$

where $L = 100$ nm is the thickness of the BHJ layer. The thickness and mobilities ($\mu_n = 1.7 \times 10^{-4}$ and $\mu_p = 7.4 \times 10^{-5}$ cm^2 V^{-1} s^{-1}, determined by fitting the *J–V* characteristics of appropriate single-carrier diodes in the scope of the space-charge-limited current model in our previous paper[12]) are known parameters. The recombination current can also be experimentally determined from the measured light and dark *J–V* curves using the following simple equations (see Figure S1, Supporting Information):

$$J_{ph} = J_L - J_d \quad (5)$$

$$J_{rec} = J_{ph.sat.} - J_{ph} \quad (6)$$

There are four unknown parameters in Equation (4): the dielectric constant of the T1:PDI bulk heterojunction layer ε, the Langevin prefactor ξ, the voltage distribution of free charge carrier density $n(V)$ and the density of deep traps N_t. Therefore, their values should be determined in order to quantify the nongeminate recombination losses in the solar cell under investigation.

It is worth noting that all measurements in this paper were carried out under constant illumination, temperature, DC bias and frequency during the measurement of each point. The amplitude of the applied AC signal was very small (10 mV) and did not change noticeably the steady state properties of the system. Thus, the system may be considered under quasi steady-state conditions at each given frequency.

2.2. AC Characteristics in the Dark

It is known that every electronic device possesses some series resistance which affects the measured capacitance at high frequencies.[34–36] The measurement of electrical and photoelectrical properties of organic BHJ solar cells is carried out in a nitrogen gloveboxes thus additional connecting wires with some inductance are used. The parasitic inductance of wires connected in series to the solar cell will also affect on the measured capacitance in the high-frequency region.[36] Therefore, the measured capacitance should be corrected by the effect of series resistance and parasitic inductance. This corrected capacitance, the actual capacitance of the BHJ layer, which is needed for the further analysis, should be calculated from the impedance spectra measured at different biases:[36]

$$C_{cor} = C_{BHJ} = -\frac{1}{\omega}\left[\frac{Z'' - \omega L_I}{(Z' - R_s)^2 + (Z'' - \omega L_I)^2}\right] \quad (7)$$

where Z' and Z'' are the real and imaginary components of the measured impedance, $L_I = 6 \times 10^{-6}$ H is the inductance of the

connecting wires and R_s is the series resistance of the solar cells and $\omega = 2\pi\nu$ is the angular frequency of the AC signal. There is a large discrepancy between the measured and corrected capacitance in the high-frequency region (Figure S2, Supporting Information). Therefore, the correction for the effect of the series resistance and the parasitic inductance is necessary, since both low- and high-frequency capacitance will be involved in the further analysis.

The capacitance of a BHJ layer consists of two components (Equation (8)): a frequency-dependent chemical capacitance C_{in}, which is originated from free charge carriers (proportional to the conductance G of the BHJ layer) (Equation (9)) and a frequency independent capacitance originated from Maxwell displacement current C_M, which may be either a voltage independent geometrical capacitance or the voltage dependent capacitance of a space charge region (Equations (10) and (11), respectively):[15,20,29,37]

$$C_{cor} = C_{BHJ} = C_{in} + C_M \tag{8}$$

$$C_{in} = qAL\frac{dn}{dV_{cor}} \propto G = \frac{dJ}{dV_{cor}} \tag{9}$$

$$C_M = C_g = \frac{\varepsilon\varepsilon_0 A}{L} \tag{10}$$

$$C_M = \frac{\varepsilon\varepsilon_0 A}{W} = A\sqrt{\frac{\varepsilon\varepsilon_0 qN}{2(V_{bi} - V_{cor})}} \tag{11}$$

where, $V_{cor} = V - JR_s$ is the applied DC voltage corrected by the effect of series resistance.

Figure 3a shows the corrected capacitance spectra of the T1:PDI SM BHJ solar cells at different applied biases in the dark. The capacitance of the BHJ layer at a large reverse bias (–2 V) is frequency independent and is equal to the geometrical capacitance C_g, since the BHJ layer is totally depleted.[15,20] The value of the dielectric constant of the BHJ blend $\varepsilon = 3.7$ can be calculated by rearranging the well-known expression for a parallel plate capacitor such that:

$$\varepsilon = \frac{C_g L}{\varepsilon_0 A} \tag{12}$$

There are three regions at low, medium, and high frequencies in Figure 3a. It is clear that the low- and high-frequency capacitance possess different voltage dependence and, thus, different physical nature. Let us consider first the high-frequency capacitance C_{HF}.

At both reverse- and small forward-biased conditions the BHJ layer is totally depleted. Therefore, C_{HF} is voltage independent and equal to the geometrical capacitance of the BHJ layer. The voltage dependence of the high-frequency capacitance follows the well-known Mott–Schottky (M–S) dependence with the further increase of forward bias (Figure 3b) that provides evidence on the voltage-dependent width of the space charge region in the BHJ layer.[20,37] According to the M–S model, the extrapolation of the linear dependence in the A^2/C^2 vs V_{cor} coordinates toward the intercept with the voltage axis gives the value of the built-in voltage $V_{bi} = 1$ V. The observed voltage dependence and

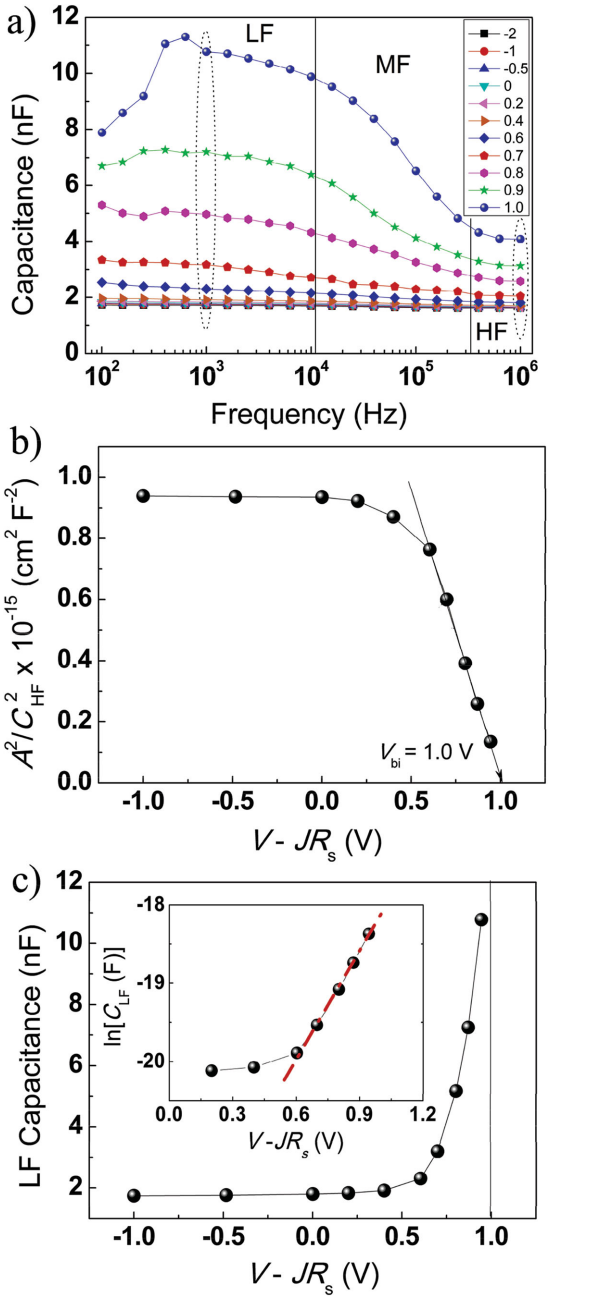

Figure 3. a) The capacitance spectra of the T1:PDI solar cell at different biases measured in the dark; b) Mott–Schottky plot of the high-frequency capacitance; c) The low-frequency capacitance vs applied bias (the inset shows the voltage dependence of the low-frequency capacitance in the semilogarithm scale).

frequency independence of the corrected capacitance in the high-frequency region show that it originates from the Maxwell displacement current. The free charge carriers cannot follow the high-frequency AC signal and therefore do not contribute to the measured capacitance.

Now let us consider the low-frequency capacitance C_{LF} vs voltage (Figure 3c). It is seen that the low-frequency capacitance exponentially increases with increasing forward bias $C_{LF} \sim \exp(V_{cor})$. This voltage dependence is similar to the voltage

dependence of the current (electrical conductivity) of the solar cell. Therefore, the low-frequency capacitance should mainly originate from the free charge carriers into the BHJ layer and is equal to the sum of the total chemical capacitance C_{in0} (all free charge carriers are able to response to the low-frequency AC signal) and frequency independent capacitance caused by the Maxwell displacement current (high-frequency capacitance). An abrupt increase in low-frequency capacitance is seen when the forward bias approaches a value of 1 V (good correlation with the previously determined value of the built-in voltage V_{bi} from the M–S plot in Figure 3b).

As a first approximation, the frequency dependence of a BHJ solar cell in the absence of traps can be described by the following equation, derived for a standard p–n homojunction solar cell (for details see Supporting Information):

$$C_{BHJ} = C_{in} + C_M \approx C_{in0} \frac{\sqrt{2}}{\sqrt{1+\sqrt{1+(\omega\tau)^2}}} + C_M \quad (13)$$

where $C_{in0} = G\tau/2$ is the total chemical capacitance (the value of the saturated chemical capacitance in the low-frequency region), τ is the time constant, which determines the response of the free charge carriers to the applied AC signal. Equation (13) quantitatively describes the frequency response of chemical capacitance in p–n homojunction solar cells and can be considered as a reference point for other types of solar cells. In order to take into account complex morphology and electrical features of organic BHJ solar cells, Equation (13) should be written in a more general form:

$$C_{BHJ} = C_{in} + C_M \approx \frac{C_{in0}}{\left(\sqrt{1+(\omega\tau)^2}\right)^{\beta}} + C_M \quad (14)$$

where the experimentally determined empirical parameter β may vary between 0.5 for p–n homojunctions and 2 for organic bilayer heterojunctions. Organic BHJ solar cells usually show $0.5 < \beta < 2$. Parameter β also depends on temperature and illumination conditions.

It is necessary to consider Equation (14) in different frequency regions, mentioned above. In the low-frequency region ($\omega\tau \ll 1$) the capacitance of the BHJ layer is determined by the sum of C_{in0} and C_M:

$$C_{BHJ} = C_{LF} = C_{in0} + C_M \quad (15)$$

In the middle frequency region ($\omega\tau \geq 1$) the capacitance of the BHJ layer is determined by the sum of the frequency-dependent chemical capacitance (the AC signal becomes faster and not all charge carriers can follow it and contribute to the measured capacitance) and the frequency independent C_M:

$$C_{BHJ} = \frac{C_{in0}}{(\omega\tau)^{\beta}} + C_M \quad (16)$$

And finally in the high-frequency region ($\omega\tau \gg 1$) the capacitance of the BHJ layer is mainly determined only by the frequency independent capacitance originating from the Maxwell displacement current $C_{BHJ} = C_{HF} = C_M$.

2.3. Capacitance Spectroscopy under Illumination and Density of Free Charge Carriers

Figure 4a shows the capacitance spectra of the T1:PDI solar cells measured under AM 1.5 100 mW cm^{-2} illumination at different applied biases. According to the aforementioned quantitative model (Equation (14)), the capacitance should saturate in the low-frequency region, decrease in the middle frequency region, and again saturate in the high-frequency region (dashed red line in Figure 4a). However, in the low-frequency region, there is some additional parasitic contribution to the capacitance from the slow processes of charging and discharging shallow traps (slight increase in capacitance with the decrease of the frequency). Shallow traps work as pure traps (the probability of detrapping is higher than that of recombination). Due to the trapping and detrapping processes (charging and discharging traps when a small amplitude AC signal is applied to a solar cell), shallow traps result in an additional capacitance, which is usually observed in a low-frequency region and decreases at high frequency. This additional frequency-dependent capacitance causes the nonideal AC characteristics of solar cells. The effect of traps on the low-frequency capacitance of the BHJ layer disserves a detailed analysis, but aim of this paper is focused on much faster processes, which are related only to free charge carriers and Maxwell displacement current. Thus, we should consider the values of the low-frequency capacitance C_{LF} at the right edge of the low-frequency region ($f \approx 17$ kHz) where all free charge carriers contribute to the capacitance and traps do not (dashed circles in Figure 4a).

The voltage distributions of the low-frequency and high-frequency capacitance under 1 sun illumination are shown in Figure 4b. The difference between them is equal to the total chemical capacitance C_{in0} originating from the free charge carriers:

$$C_{in0} = C_{LF} - C_{HF} \quad (17)$$

Taking into account the expression for the chemical capacitance (Equation (9)), the density of free charge carriers as a function of applied bias can be calculated using the equation:[15,38]

$$n(V_{cor}) = n_{sat} + \frac{1}{qAL}\int_{V_{sat}}^{V_{cor}} C_{in0}\, dV_{cor} \quad (18)$$

where V_{sat} is the reverse bias at which the photocurrent saturates. Assuming that at V_{sat}, the generation rate is constant and recombination losses are negligible due to the strong internal electric field, n_{sat} can be calculated as follows:[15]

$$n_{sat} = \frac{1}{qAL} C_{sat}(V_0 - V_{sat}) \quad (19)$$

where C_{sat} is the capacitance of the BHJ layer under illumination at V_{sat} and V_0 is the forward bias at which the photocurrent is equal to zero (see Figure S1, Supporting Information). The

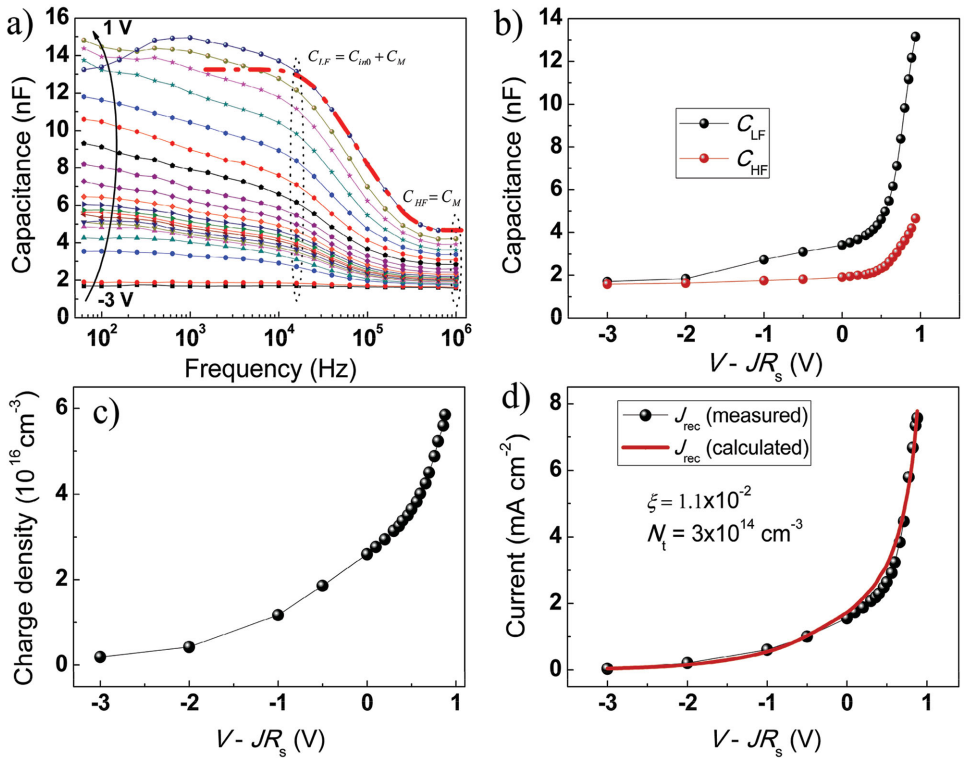

Figure 4. a) The capacitance spectroscopy of the T1:PDI solar cell under 1.5 AM 100 mW cm^{-2} illumination (the dashed circles denote the considered low and high capacitance and the dashed red line shows the theoretically predicted capacitance spectroscopy); b) The voltage dependence of the high- and low-frequency capacitance; c) The voltage dependence of the density of free charge carriers in the BHJ layer; d) The experimentally measured and fitted recombination current under 1.5 AM 100 mW cm^{-2} illumination. The value of the series resistance R_s was determined under illumination (Figure S3, Supporting Information).

calculated density of free charge carriers in the BHJ layer as a function of applied bias, corrected by the voltage drop over the series resistance, is shown in Figure 4c. The calculated density of free charge carriers is similar to that reported for other small-molecule systems under 1 Sun illumination.[15]

2.4. Measured and Calculated Recombination Current

Having determined the dielectric constant and the density of free charge carriers using Equations (12) and (17), respectively, we can go further in the analysis of the nongeminate recombination losses in the T1:PDI SM BHJ solar cell. The experimentally determined recombination current is shown by black circles in Figure 4d. The last two unknown parameters in Equation (4), the Langevine prefactor (ξ) and density of deep traps (N_t) can be considered as fitting parameters in order to describe quantitatively the experimental recombination current in the scope of the bimolecular and SRH recombination models. Based on the best fitting between the experimental and calculated curves (see Figure 4d), values of the unknown parameters were determined to be $\xi = 1.1 \times 10^{-2}$ and $N_t = 3 \times 10^{14}$ cm^{-2}.

Now it is possible to distinguish between the contributions of both the bimolecular and the SRH recombination mechanisms toward the total nongeminate recombination losses in the T1:PDI SM BHJ solar cell. **Figure 5**a shows the total recombination current, which is the superposition of the bimolecular and SRH recombination currents. It is seen that different recombination mechanisms dominate at different bias. SHR recombination dominates at reverse biases when the recombination current is very small due to the low density of free charge carriers. However, the contribution of bimolecular recombination strongly increases with the increase of forward bias and mainly determines the recombination losses at open circuit conditions when the density of free charge carriers in the BHJ layer is the highest. The inset in Figure 5a shows the ratio between the bimolecular and SRH recombination currents vs applied voltage for the T1:PDI solar cell.

It is very important that the contribution of different recombination mechanisms can be considered separately. Bimolecular recombination is always present in an organic BHJ layer. However, SRH recombination is observed only in the presence of deep traps. Thus, theoretically, the recombination losses due to SRH recombination can be eliminated by the decrease of the density of deep traps N_t. Since the contribution of SRH recombination has been quantified, it can be subtracted from the total recombination current in order to estimate the losses of the main photoelectrical parameters of the solar cell caused by the presence of deep traps in the T1:PDI SM BHJ solar cell (Figure 5b). Here the black line shows the measured J–V curve under one sun illumination. The red line shows the J–V curve obtained by the subtraction of the SRH recombination losses. It is seen that SRH recombination in the solar cell under investigation mainly decreases the short-circuit current by 7%

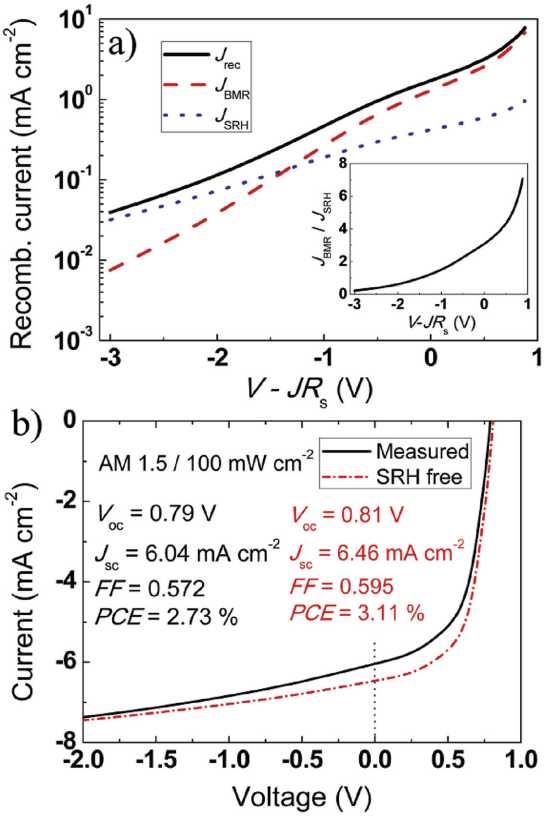

Figure 5. a) The total recombination current as a superposition of the bimolecular and SRH recombination currents vs applied bias. The inset shows the voltage dependence of the ratio between the bimolecular and SRH recombination currents; b) The effect of the SRH recombination on the main photoelectrical parameters of the T1:PDI solar cell.

relatively to its measured value and also slightly decreases V_{oc} and *FF* by 2.5% and 4%, respectively. The relative decrease in the PCE by 14% is observed due to the presence of trap-assisted recombination.

3. Conclusions

A new approach for the determination of the density of free charge carriers in the organic BHJ solar cells under illumination as a function of applied bias using capacitance spectroscopy is proposed. This approach was used to quantitatively analyze the nongeminate recombination losses in the nonfullerene T1:PDI SM BHJ solar cell system under standard illumination conditions (AM 1.5, 100 mW cm^{-2}). Using this approach, the losses due to bimolecular and trap-assisted recombination were calculated separately, thereby revealing the individual contributions of each loss mechanism at different applied bias conditions. This analysis revealed that trap-assisted recombination is most prevalent at reverse bias conditions while bimolecular recombination dominates at forward bias conditions. The decrease in the PCE of T1:PDI solar cells directly attributable to trap-assisted recombination was found to be 14% relative to its measured value (≈0.4% in absolute value). Thus, the further improvement of the T1:PDI solar cells should be focused on the decreasing the geminate and bimolecular recombination losses. The decrease of the SRH recombination should be considered as a secondary optimization step, since these findings indicate that it is a relatively minor loss mechanism in the nonfullerene T1:PDI system. However, this may not be the case for other BHJ systems especially those fabricated from materials containing impurities. Furthermore, we posit that the approach presented here for measuring and interpreting the frequency-dependent capacitance of operating solar cells may be widely applied to identify and quantify recombination losses in BHJ solar cells.

4. Experimental Section

ITO substrates purchased from Thin Film Devices, Inc. were cleaned by detergent, DI water, acetone, and isopropanol with ultrasonication for 30 min, sequentially. The hole transport layer of poly(3,4-ethylenedioxythiophene) poly(styrenesulfonate) (PEDOT:PSS) (Clevious PH) was spin-cast at 2500 rpm for 60 s and annealed at 140 °C in air for 30 min. The solution of T1 and PDI was prepared in a 1:1 weight ratio at a total solids concentration of 30 mg mL^{-1} in chlorobenzene with 0.4 vol% diiodooctane (DIO) processing additive. The solution was stirred and heated overnight at 120 °C and cooled down to 90 °C prior to spin casting at 1500 rpm for 60 s. The thickness of the BHJ layers was measured by an Ambios XP-100 stylus profilometer to be ≈100 nm. Then, a 5 nm calcium layer was deposited on top of the BHJ layer. Afterward, a 100 nm aluminium cathode was thermally deposited at a pressure of 4×10^{-6} Torr. The total cell area was 5 mm^2. A schematic representation of the solar cells is shown in Figure S4 (Supporting Information).

The current–voltage (*J*–*V*) characteristics as well as the spectral distributions of the real and imaginary components of the impedance of the T1:PDI solar cells were measured by an impedance analyzer Solartron SI 1255, SI 1287 in the dark and under illumination. The small amplitude AC signal (10 mV) was applied to prevent the effect of the AC signal on the measured impedance. The light source was an AM1.5 solar simulator (300 W Xe arc lamp with an AM 1.5 global filter). Solar simulator irradiance was calibrated using a standard silicon photovoltaic cell with a protective KG1 filter calibrated by the National Renewable Energy Laboratory.

Supporting Information

Supporting Information is available from the Wiley Online Library or from the author.

Acknowledgements

V.V.B and C.M.P. thank the Office of Naval Research (Award No. N00014-14-1-0076) for support of this work. N.A.R. thanks the Office of Naval Research (Award No. N00014-14-1-0580). T.Q.N. thanks the Camille Dreyfus Teacher Scholar Award. The authors thank Dr. Alexander Sharenko (Stanford University), Samuel Collins, Nickolas Lee and Ben Luginbhl (UCSB) for useful discussions.

Received: November 11, 2015
Revised: February 18, 2016
Published online: March 29, 2016

[1] A. J. Heeger, *Adv. Mater.* **2014**, *26*, 10.
[2] A. K. Rath, M. Bernechea, L. Martinez, F. P. G. de Arquer, J. Osmond, G. Konstantatos, *Nat. Photonics* **2012**, *6*, 529.

[3] Y. Sun, G. C. Welch, W. L. Leong, C. J. Takacs, G. C. Bazan, A. J. Heeger, *Nat. Mater.* **2012**, *11*, 44.
[4] B. Walker, C. Kim, T.-Q. Nguyen, *Chem. Mater.* **2011**, *23*, 470.
[5] B. Kan, Q. Zhang, M. Li, X. Wan, W. Ni, G. Long, Y. Wang, X. Yang, H. Feng, Y. Chen, *J. Am. Chem. Soc.* **2014**, *136*, 15529.
[6] X. Guo, M. Zhang, W. Ma, L. Ye, S. Zhang, S. Liu, H. Ade, F. Huang, J. Hou, *Adv. Mater.* **2014**, *26*, 4043.
[7] A. Maurano, R. Hamilton, C. G. Shuttle, A. M. Ballantyne, J. Nelson, B. O'Regan, W. Zhang, I. McCulloch, H. Azimi, M. Morana, C. J. Brabec, J. R. Durrant, *Adv. Mater.* **2010**, *22*, 4987.
[8] L. Lu, L. Yu, *Adv. Mater.* **2014**, *26*, 4413.
[9] A. Anctil, C. W. Babbitt, R. P. Raffaelle, B. J. Landi, *Environ. Sci. Technol.* **2011**, *45*, 2353.
[10] J. T. Bloking, T. Giovenzana, A. T. Higgs, A. J. Ponec, E. T. Hoke, K. Vandewal, S. Ko, Z. Bao, A. Sellinger, M. D. McGehee, *Adv. Energy Mater.* **2014**, *4*, 1301426.
[11] C. Li, H. Wonneberger, *Adv. Mater.* **2012**, *24*, 613.
[12] A. Sharenko, C. M. Proctor, T. S. van der Poll, Z. B. Henson, T.-Q. Nguyen, G. C. Bazan, *Adv. Mater.* **2013**, *25*, 4403.
[13] A. Sharenko, D. Gehrig, F. Laquai, T.-Q. Nguyen, *Chem. Mater.* **2014**, *26*, 4109.
[14] R. J. Chesterfield, J. C. McKeen, C. R. Newman, P. C. Ewbank, D. A. da Silva Filho, J.-L. Brédas, L. L. Miller, K. R. Mann, C. D. Frisbie, *J. Phys. Chem. B* **2004**, *108*, 19281.
[15] C. M. Proctor, C. Kim, D. Neher, T.-Q. Nguyen, *Adv. Funct. Mater.* **2013**, *23*, 3584.
[16] E. Barsoukov, J. R. Macdonald, *Impedance Spectroscopy: Theory, Experiment, and Applications*, Wiley, Hoboken **2005**.
[17] V. V. Brus, *Semicond. Sci. Technol.* **2013**, *28*, 025013.
[18] V. V. Brus, M. Zellmeier, X. Zhang, S. M. Greil, M. Gluba, A. J. Töfflinger, J. Rappich, N. H. Nickel, *Org. Electron.* **2013**, *14*, 3109.
[19] F. Fabregat-Santiago, G. Garcia-Belmonte, I. Mora-Seró, J. Bisquert, *Phys. Chem. Chem. Phys.* **2011**, *13*, 9083.
[20] M. Mingebach, C. Deibel, V. Dyakonov, *Phys. Rev. B* **2011**, *84*, 153201.
[21] G. A. H. Wetzelaer, M. Kuik, M. Lenes, P. W. M. Blom, *Appl. Phys. Lett.* **2011**, *99*, 153506.
[22] R. A. Street, M. Schoendorf, A. Roy, J. H. Lee, *Phys. Rev. B* **2010**, *81*, 205307.
[23] V. V. Brus, A. K. K. Kyaw, P. D. Maryanchuk, J. Zhang, *Org. Electron.* **2014**, *15*, 2141.
[24] R. Yatskiv, V. V. Brus, M. Verde, J. Grym, P. Gladkov, *Carbon* **2014**, *77*, 1011.
[25] L. J. A. Koster, V. D. Mihailetchi, R. Ramaker, P. W. M. Blom, *Appl. Phys. Lett.* **2005**, *86*, 123509.
[26] M. M. Mandoc, W. Veurman, L. J. A. Koster, B. de Boer, P. W. M. Blom, *Adv. Funct. Mater.* **2007**, *17*, 2167.
[27] S. R. Cowan, A. Roy, A. J. Heeger, *Phys. Rev. B* **2010**, *82*, 245207.
[28] R. Mauer, I. A. Howard, F. Laquai, *J. Phys. Chem. Lett.* **2010**, *1*, 3500.
[29] S. M. Sze, K. K. Ng, *Physics of Semiconductor Devices*, Wiley, Hoboken **2007**.
[30] S. R. Cowan, W. L. Leong, N. Banerji, G. Dennler, A. J. Heeger, *Adv. Funct. Mater.* **2011**, *21*, 3083.
[31] C. M. Proctor, M. Kuik, T.-Q. Nguyen, *Prog. Polym. Sci.* **2013**, *38*, 1941.
[32] M. Kuik, L. J. A. Koster, G. A. H. Wetzelaer, P. W. M. Blom, *Phys. Rev. Lett.* **2011**, *107*, 256805.
[33] M. Kuik, G.-J. A. H. Wetzelaer, H. T. Nicolai, N. I. Craciun, D. M. De Leeuw, P. W. M. Blom, *Adv. Mater.* **2014**, *26*, 512.
[34] A. S. Kavasoglu, N. Kavasoglu, S. Oktik, *Solid State Electron.* **2008**, *52*, 990.
[35] V. V. Brus, *Semiconductors* **2012**, *46*, 1012.
[36] V. V. Brus, *Semicond. Sci. Technol.* **2012**, *27*, 035024.
[37] G. F. A. Dibb, M.-A. Muth, T. Kirchartz, S. Engmann, H. Hoppe, G. Gobsch, M. Thelakkat, N. Blouin, S. Tierney, M. Carrasco-Orozco, J. R. Durrant, J. Nelson, *Sci. Rep.* **2013**, *3*, 03335.
[38] G. Garcia-Belmonte, P. P. Boix, J. Bisquert, M. Sessolo, H. J. Bolink, *Sol. Energy Mater. Sol. Cells* **2010**, *94*, 366.

ADVANCED ENERGY MATERIALS

Supporting Information

for *Adv. Energy Mater.,* DOI: 10.1002/aenm.201502250

Capacitance Spectroscopy for Quantifying Recombination Losses in Nonfullerene Small-Molecule Bulk Heterojunction Solar Cells

*Viktor V. Brus, Christopher M. Proctor, Niva A. Ran, and Thuc-Quyen Nguyen**

Supporting Information

Capacitance Spectroscopy for Quantifying Recombination Losses in Non-Fullerene Small-Molecule Bulk-Heterojunction Solar Cells

Viktor V. Brus[*]*, Christopher M. Proctor, Niva A. Ran, Thuc-Quyen Nguyen*[*]

Dr. V.V. Brus, Dr. C. M. Proctor, Niva A. Ran, Prof. T.-Q. Nguyen
Center for Polymers and Organic Solids, Department of Chemistry and Biochemistry, University of California at Santa Barbara, Santa Barbara, CA, 93106, USA

Prof. T.-Q. Nguyen
Department of Chemistry, Faculty of Science, King Abdulaziz University, Jeddah, Saudi Arabia

[*]Email: vbrus@chem.ucsb.edu, quyen@chem.ucsb.edu

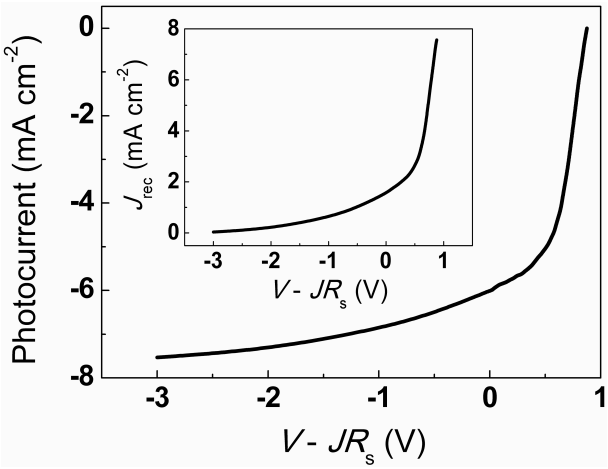

Figure S1. Photocurrent and recombination current of the T1:PDI solar cell determined from the J-V curves measured in the dark and under AM 1.5 100 mW cm^{-2} illumination.

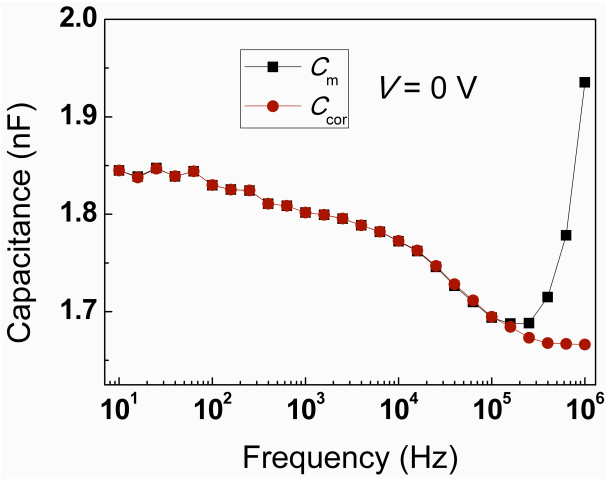

Figure S2. The comparison of the measured and corrected by the effect of series resistance and parasitic inductance capacitance spectroscopy of the T1:PDI solar cell in the dark at zero bias.

A quantitative model for the AC signal response of a solar cell

If a superposition of the DC bias and small AC signal is applied to a solar cell:

$$V(t) = V_0 + \Delta V \exp(i\omega t), \tag{1}$$

where V_0 is the applied DC voltage and ΔV is the amplitude of the small AC signal, ω is the angular frequency of the small AC signal, t is time, the resultant current density will be given by the next equation:[1-3]

$$J(t) = J_0 + \Delta J \exp(i\omega t), \tag{2}$$

where J_0 is the DC component, and $\Delta J = \Delta J_{n,p} + \Delta J_M$ is the sum of the amplitudes of the current density caused by the transport of free charge carriers in the BHJ layer $\Delta J_{n,p}$ and the Maxwell displacement current ΔJ_M, caused by the change of the electric field:[4]

$$\Delta J_M \exp(i\omega t) = \varepsilon\varepsilon_0 \frac{\partial E}{\partial t}, \tag{3}$$

where ε is the dielectric constant, ε_0 is the permittivity of free space, E is the strength of the electric field.

The admittance (complex conductance) generally can be determined as follows:

$$Y = \frac{1}{Z} = \frac{\Delta J}{\Delta V} = \frac{\Delta J_{n,p}}{\Delta V} + \frac{\Delta J_M}{\Delta V}, \tag{4}$$

where Z is the impedance.

The admittance of the solar cell in the presence of free charge carriers (photo-induced and injected from electric contacts) and in the absence of electrically active traps can be described by the next equation:[1-3]

$$Y = \frac{1}{Z} \approx G\sqrt{1 + i\omega\tau} + i\omega C_M, \tag{5}$$

where G is the DC conductance, which is reversely proportional to the differential resistance R_{diff}:

$$G = \frac{dJ_0}{dV_{cor}} = \frac{1}{R_{diff}}. \tag{6}$$

Having used the Moivre's formula:[3]

$$\sqrt{1+i\omega\tau} = \frac{\sqrt{1+\sqrt{1+(\omega\tau)^2}}}{\sqrt{2}} + i\frac{\omega\tau}{\sqrt{2}\sqrt{1+\sqrt{1+(\omega\tau)^2}}}, \tag{7}$$

Equation (5) can be transformed to show the real and imaginary components of the admittance:

$$Y = \frac{1}{Z} = G\frac{\sqrt{1+\sqrt{1+(\omega\tau)^2}}}{\sqrt{2}} + i\omega\left[\frac{G\tau}{\sqrt{2}\sqrt{1+\sqrt{1+(\omega\tau)^2}}} + C_M\right] = G_{BHJ} + i\omega C_{BHJ}, \tag{8}$$

It is seen from the imaginary part of Equation (8) that the capacitance is governed by the following equation:

$$C_{BHJ} = C_{cor} = \frac{G\tau}{\sqrt{2}\sqrt{1+\sqrt{1+(\omega\tau)^2}}} + C_M, \tag{9}$$

Equation (9) can be written in other form:

$$C_{BHJ} = C_{in0}\frac{\sqrt{2}}{\sqrt{1+\sqrt{1+(\omega\tau)^2}}} + C_M, \tag{10}$$

where $C_{in0} = G\tau/2$ is the saturated chemical capacitance in the low frequency region.

The described capacitance model was derived for an ideal p-n-homojunction (1 - electrical contacts are ideally ohmic; 2 - surface effect is negligible; 3 - absence of traps...). Unfortunately, BHJ solar cells do not meet all of these requirements in full extent and the development of an analytical model for chemical capacitance which takes into account all of the possible non-idealities in BHJ solar cells is too complicated to be carried out. However, the main AC characteristics of the BHJ solar cells possess very similar features with that of p-n-homojunctions: frequency dependent and exponentially voltage dependent chemical capacitance due to the contribution of free charge carriers as well as frequency independent

Maxwell displacement current capacitance (capacitance of the depletion region). This fact shows that the considered analytical model can be used for the analysis of capacitance spectra of BHJ solar cells in first approximation. Afterward, we empirically modified the theoretically derived equation, which describes the frequency dependence of the capacitance of p-n-homojunctions based on experimentally measured capacitance spectra of different organic BHJ and bi-layer solar cells (Equation 14 in the main text). One of the aims of our paper is to propose a relatively simple practically applicable approach for the quantitative estimation of main recombination losses in BHJ solar cells.

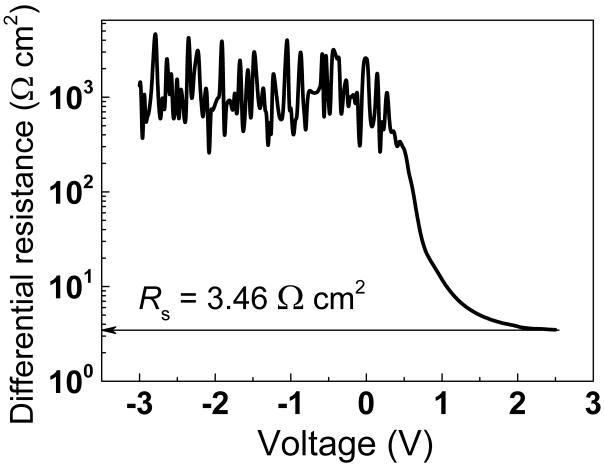

Figure S3. Voltage dependence of the differential resistance of the solar cell und 1 Sun illumination.

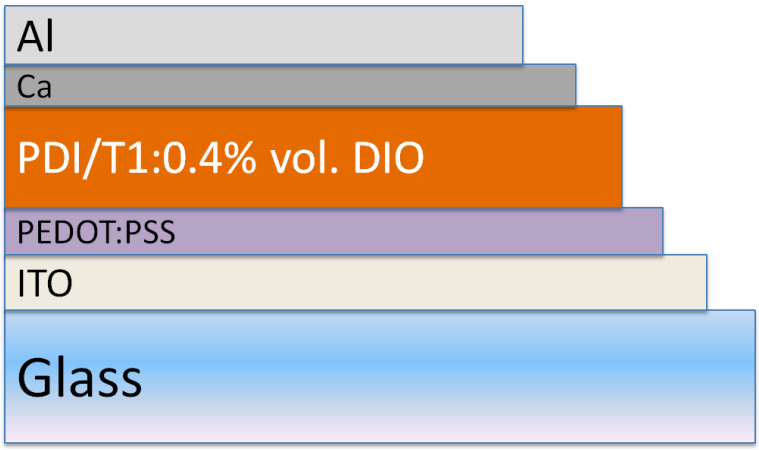

Figure S4. The schematic representation of the non-fullerene SM BHJ T1:PDI solar cell under investigation.

[1] S. M. Sze, K. K. Ng, *Physics of Semiconductor Devices*, Wiley, NJ, USA **2007**.

[2] V. V. Pasynkov, L.K. Chirkin, *Semiconductor Devices*, Vyshaya shkola, Moscow, USSR **1987** (in Russian)**.**

[3] V. I. Strikha, *Contact Phenomena in Semiconductors*, Vyscha shkola, Kiev, USSR **1982** (in Russian).

[4] J. D. Jackson, *Classical Electrodynamics*, Wiley, NY, USA **1999**.